IEEE Access
Multidisciplinary | Rapid Review | Open Access Journal

Received March 9, 2019, accepted March 28, 2019, date of publication April 24, 2019, date of current version June 4, 2019.

Digital Object Identifier 10.1109/ACCESS.2019.2911693

Range Coherence Factor for Down Range Sidelobes Suppression in Radar Imaging Through Multilayered Dielectric Media

QIANG AN[1,2], AHMAD HOORFAR[2], (Senior Member, IEEE), WENJI ZHANG[2], SHIYONG LI[3], (Member, IEEE), AND JIANQI WANG[1]

[1]Department of Biomedical Engineering, Fourth Military Medical University, Xi'an 710032, China
[2]Antenna Research Laboratory, Center for Advanced Communications, Villanova University, Villanova, PA 19085, USA
[3]Beijing Key Laboratory of Millimeter Wave and Terahertz Technology, Beijing Institute of Technology, Beijing 100081, China

Corresponding author: Jianqi Wang (wangjq@fmmu.edu.cn)

This work was supported in part by the National Key R&D Program of China under Grant 2018YFC0810201, and in part by the National Natural Science Foundation of China under Grant 31800822 and Grant 81601567.

ABSTRACT In radar imaging applications through layered dielectric media, an antenna array with a limited operating frequency bandwidth at the low end of the microwave band is usually employed to probe the target space of interests. As a result, the focused radar imagery is characterized by severe sidelobes in the down-range direction, which leads to the degradation of the image quality. Several techniques, such as windowing and apodization filtering combined with phase coherence factor (PCF) filtering, have been reported to suppress the down-range sidelobes. However, these approaches either expand the main lobe width or are sensitive to parameter tuning. In this paper, by investigating the distribution characteristics of the down-range sidelobes among sub-frequency radar imageries, a robust and efficient range coherence factor (rCF) technique is proposed to suppress the down-range sidelobes in the focused radar imagery. The performance of the proposed approach is assessed by the finite-difference time-domain (FDTD)-based numerical simulations as well as onsite experiments to verify its sidelobes' reduction capabilities.

INDEX TERMS Down range sidelobes, finite-difference time-domain (FDTD), ground penetrating radar (GPR), lateral grating lobes, Range coherence factor (rCF), through-the-wall radar imaging (TWRI).

I. INTRODUCTION

Radar imaging of obscured targets of interest behind wall or buried underneath has long been a research focus in microwave imaging community, especially for ground penetrating radar (GPR) and through-the-wall wall radar imaging (TWRI) applications. Accurate targets detection and localization would provide the potential operators with authentic information about the environment under investigation, which would assist the operators in making decision prior to the operation being carried out [1], [2].

To achieve the rapid intelligent sensing, a linear inverse scattering model based on Born approximation is often adopted to alleviate the computation burden and accelerate the imaging process [3]–[7]. However, due to practical limitations when deploying a real radar system onsite, mainly the restricted deployment locations and cost efficient requirement, we usually just have access to a very limited number of transceiving antenna elements. Then, when synthesizing the scattered field along the aperture dimension, insufficient spatial sampling would definitely introduce strong lateral grating lobes in the focused radar imagery. Numerous approaches, such as aperture windowing [8], channel weighting through convex optimization [9], [10], CLEAN algorithm [11], [12], coherence factor (CF) filtering [13]–[15], phase coherence factor (PCF) filtering [16]–[18], sign coherence factor (SCF) filtering [19] and power spectrum coherence factor (PSCF) filtering [20], have been reported to suppress the grating lobes, in which the CF filtering approach has been proved to effectively suppress the grating lobes of the sparse array for TWRI.

Apart from the lateral grating lobes introduced by a sparse array, for a real radar system operating onsite for TWRI and GPR imaging purpose, it is often the case that a sequence

The associate editor coordinating the review of this manuscript and approving it for publication was Avishek Guha.

of frequency samples around the L-band (1.0-2.0GHz) is employed to scan the region of interest in order to satisfy the required electromagnetic wave penetration ability [1]. As a result, the reconstructed target scene will be surely corrupted by severe sidelobes in down range direction because of the discontinuity of the spectrum.

In general, range windowing is the most commonly adopted approach to suppress down range sidelobes, including triangular, Hanning, Kaiser and Blackman windows [21]. The drawback of the approach is obvious in that it expands the width of the mainlobe and raises the grating lobes level [22]. Subsequently, a method based on PCF combined with dual apodization was introduced to combat the down range sidelobes while preserving the mainlobe width [23]. However, the performance of the method relies highly on the choice of the constant in PCF formula. Lately, a spatial spectrum segmentation approach was proposed to reduce the down range sidelobes and simultaneously keep the mainlobe width [24]. Although the method is easy to implement, its sidelobes suppression capability relies heavily on spectrum division strategies.

In this paper, we propose a range coherence factor (rCF) filtering approach to suppress the down range sidelobes. The approach first measures the coherence levels for each pixel in target space among sub-frequency radar imageries. By employing a similar incoherent summation as CF did along frequency dimension rather than aperture dimension, an rCF map is produced. Then, by filtering the direct focused radar imagery with the above rCF map, the down range sidelobes can be suppressed effectively.

The rest of the paper is organized as follows. In section 2, the inverse scattering model and the beamforming algorithm for radar imaging through layered GPR are detailed. In section 3, the CF filtering approach is reviewed and the formulation for rCF is introduced. In section 4, numerical examples for both GPR and TWRI are provided to evaluate the performance of the proposed down range sidelobes suppression method. In Section 5, a TWRI experiment for detection of multiple behind wall stationary human targets is conducted to further verify the effectiveness of the proposed approach. In Section 6, the concluding remarks are provided.

II. RADAR IMAGING MODEL FOR THROUGH LAYERED DIELECTRIC MEDIA

Consider a typical 2-D multiple-input multiple-output (MIMO) GPR imaging through two layered subsurface ground geometry as depicted in Fig. 1.

A target with an arbitrary shape is buried in the second layer of the investigation domain D. An antenna array operating in a multi-static mode is utilized to probe the target space. The positions of transmitters and receivers are denoted by r_{tn} and r_{rm}, respectively. Under the point target model assumption, the received signal can be written as below,

$$E_s\left(r_{rm}, r_{tn}, k_p\right) = \int dr\sigma\left(r\right) G\left(r_{rm}, r, k_p\right) G\left(r, r_{tn}, k_p\right) \quad (1)$$

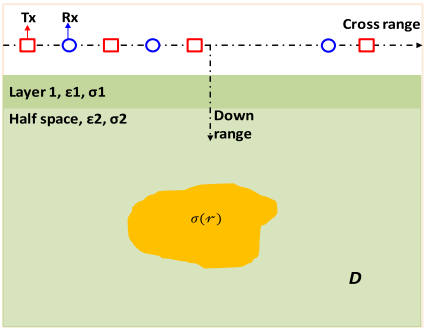

FIGURE 1. 2-D GPR imaging geometry.

where $E_s(r_{rm}, r_{tn}, k_p)$ denotes the collected scattered field at all antenna locations and frequency bins. $\sigma(r)$ denotes the target reflectivity. $G(r, r_{tn}, k_p)$ and $G(r_{rm}, r, k_p)$ represent the layered subsurface Green's functions [5], which model the subsurface EM wave propagation from transmitter to target and from target to receiver, respectively. For GPR applications, the multilayered subsurface Green's functions can be derived in closed-form and efficiently evaluated using saddle-point method [32].

The subsurface target space can then be reconstructed through the following adjoint operation [31],

$$I\left(r\right) = \sum_{m=1}^{M}\sum_{n=1}^{N}\sum_{p=1}^{P} E_s\left(r_{rm}, r_{tn}, k_p\right) \cdot G^*\left(r_{rm}, r, k_p\right) G^*\left(r, r_{tn}, k_p\right) \quad (2)$$

where M, N and P are the total number of receivers, transmitters and frequency bins, respectively.

Given the scattered field at all antenna locations, the target space can be recovered with high fidelity using the equation in (2). However, in a real GPR imaging application, severe lateral grating lobes and down range sidelobes often characterize the reconstructed underground scene as discussed above. Since effective approaches like CF filtering have been reported to account for the grating lobes, we only consider in this paper the ways to suppress the down range sidelobes.

III. PROPOSED SIDELOBES SUPPRESSION STRATEGIES

A. COHERENCE FACTOR FILTERING FOR CROSS RANGE SIDELOBES SUPPRESSION

The CF filtering was originally applied in medical ultrasound imaging to suppress the clutters in ultrasonic imageries [25]. The radar community borrowed the concept and proved its excellent performance in suppressing multipath ghosts [26], [27], grating lobes [13], sidelobes [28] and other kinds of clutters [14], [29] in a radar imagery through extensive numerical and experimental investigations. In this work, we only focus on its grating lobes suppression capability.

In the CF approach, P frequency samples of each transceiving channel is first coherently integrated together to obtain a

sub-channel radar imagery as below,

$$I_{mn}(r) = \sum_{p=1}^{P} E_s\left(r_{rm}, r_{tn}, k_p\right) \cdot G^*\left(r_{rm}, r, k_p\right) G^*\left(r, r_{tn}, k_p\right) r \in D \quad (3)$$

where $mn = 1, \ldots, MN$. Since we have a total number of MN equivalent channels, we could obtain MN sub-channel images.

Then, the CF, which is defined as the ratio of the coherence power to the incoherence power for a generic point in target space D [30], can be formulated as follows,

$$CF(r) = \frac{\left|\sum_{mn=1}^{MN} I_{mn}(r)\right|^2}{MN \sum_{mn=1}^{MN} |I_{mn}(r)|^2} \quad r \in D \quad (4)$$

By repeating the above process for each pixel in reconstruction domain, a CF map, with values varying from zero to one, is readily available. The CF map describes the coherence distribution of the target space, in which regions corresponding to targets are with values near to one, while regions corresponding to grating lobes have values near to zero.

After a pixel-by-pixel multiplication of the direct focused radar imagery I with the above CF map, a CF filtered radar imagery I_{CF} is given as below,

$$I_{CF}(r) = CF(r) \cdot I(r) \quad r \in D \quad (5)$$

where denotes the dot product. In this way, the grating lobes will be significantly attenuated.

However, the CF can only reduce the grating lobes. It's unable to suppress the down range sidelobes, as we will show later through numerical simulation examples.

B. PROPOSED RANGE COHERENCE FACTOR FILTERING FOR DOWN RANGE SIDELOBES SUPPRESSION

In this part, we continue to investigate how to suppress the down range sidelobes caused by the discontinuity of operational frequencies.

Inspired by the targets and grating lobes distribution variation among sub-channel radar imageries, which has been discussed extensively in CF based grating lobes suppression literatures, it should be anticipated that the targets and down range sidelobes will exhibit a similar coherence variation among sub-frequency radar imageries since different backscattered frequency samples carry slightly different information about the underground target space.

Assuming the underground scene keeps the same as in Fig. 1, we first define a sub-frequency radar imagery as below,

$$I_p(r) = \sum_{m=1}^{M} \sum_{n=1}^{N} E_s\left(r_{rm}, r_{tn}, k_p\right) \cdot G^*\left(r_{rm}, r, k_p\right) G^*\left(r, r_{tn}, k_p\right) \quad r \in D \quad (6)$$

where $p = 1, \ldots, P$.

The above image is obtained by integrating the scattered field of all transceiving channels for frequency p. Since we have P frequency bins in total, P such sub-frequency images will be generated in this way.

Then, a range coherence factor (rCF), which aims to measure the coherence distribution of the underground target space from sub-frequency radar imageries, is defined as follows,

$$rCF(r) = \frac{\left|\sum_{p=1}^{P} I_p(r)\right|^2}{P \sum_{p=1}^{P} \left|I_p(r)\right|^2} \quad r \in D \quad (7)$$

By employing a similar multiplication procedure, an rCF filtered radar imagery can be formulated as below,

$$I_{rCF}(r) = rCF(r) \cdot I(r) \quad r \in D \quad (8)$$

in which down range sidelobes are ideally suppressed.

Numerical examples will be presented in the following section to demonstrate the effectiveness of the proposed down range sidelobes suppression technique.

IV. NUMERICAL RESULTS

A. GPR IMAGING EXAMPLES

In the first example, we investigate the down range sidelobes suppression performance of the proposed technique for three targets buried under a two-layered subsurface ground.

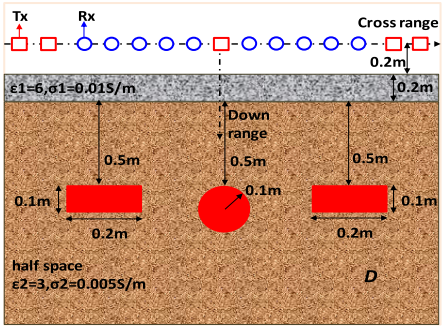

FIGURE 2. Simulation geometry for GPR imaging of three targets buried under multilayered ground.

The simulation geometry is depicted as in Fig. 2. The permittivity, conductivity and thickness of the first ground layer are $\varepsilon_{r1} = 6$, $\sigma_1 = 0.01$ S/m and $d = 0.2$ m, respectively. Three metallic targets, from left to right, rectangular, cylindrical and rectangular, are buried in the half-space layer with the permittivity $\varepsilon_{r2} = 3$ and conductivity $\sigma_2 = 0.005$ S/m. A sparse antenna array, composed of 5 transmitters and 10 receivers located 0.2 m from the upper surface of the top layer, is employed to collect the scattered field. The antenna system works at a frequency band ranging from 800 MHz to 2 GHz, covering 49 equally spaced frequency bins.

Fig. 3 a (1)-a (3) show the sub-channel radar imageries, focused using equation (3), for equivalent channel 1, 25 and 50, respectively. As can be observed, only a small portion of the three targets is recovered in each sub-channel image,

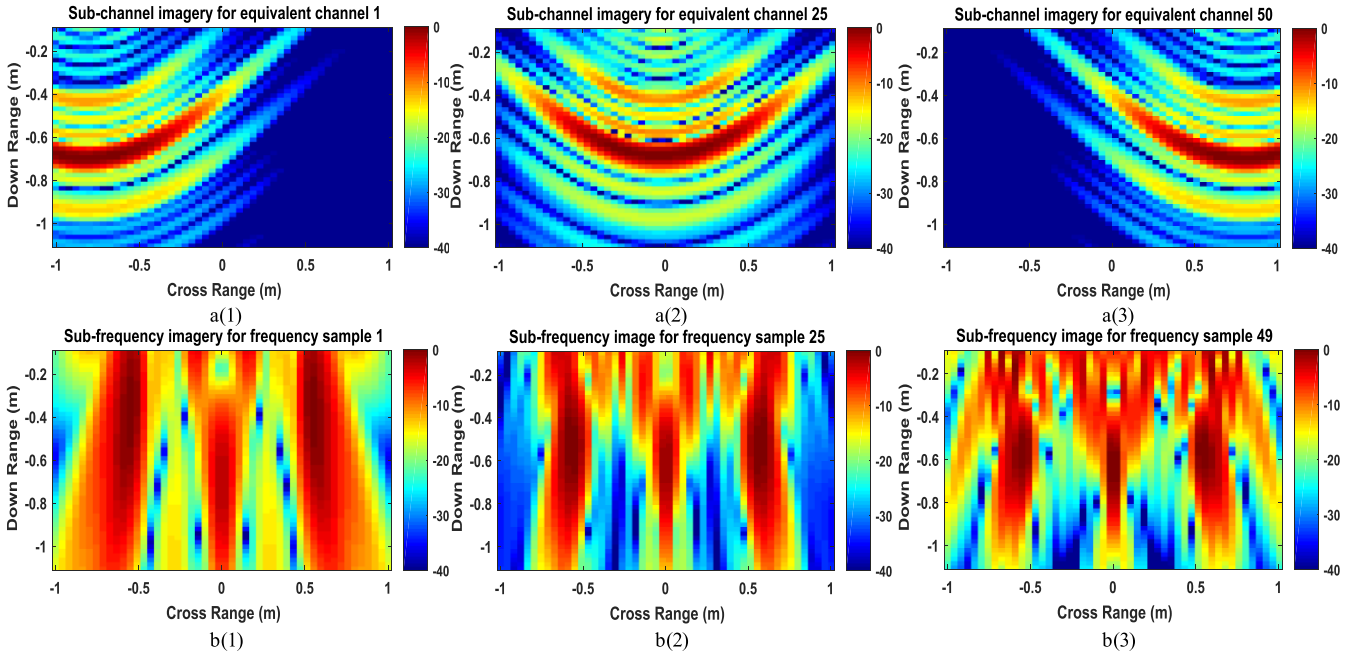

FIGURE 3. Sub-channel and sub-frequency radar imageries for three targets buried under two layered subsurface ground as depicted in Fig. 2. (a1-a3) Sub-channel radar images for equivalent channel 1, 25 and 50, respectively. (b1-b3) Sub-frequency radar imageries for frequency sample 1, 25 and 49.

which is caused by the restricted available observation angle for each transceiving channel. At the same time, the reconstructed scene is populated with severe lateral grating lobes because of insufficient cross range sampling, since only one channel data is utilized to focus the sub-channel image. These grating lobes exhibit an obvious aspect dependent characteristic across the sub-channel images, while the down range sidelobes do not. Instead, they present a similar repetition pattern in these sub-channel images, which implies that the coherence level for the down range sideloebs would be high in the CF map. Fig. 4 (a) shows the corresponding CF map obtained using equation (4), in which the coherence level for the grating lobes is greatly reduced, while those of the targets and down range sidelobes are high. The result is in agreement with our analysis. Then, after applying the CF filtering, the grating lobes will be suppressed, while the targets will be enhanced. However, the CF approach is unable to suppress the down range sidelobes.

Fig. 3 b (1)-b (3) show the sub-frequency radar imageries focused through equation (6) for frequency sample 1, 25 and 49, respectively. Three targets are clearly discriminable in cross range direction, while severe down range sidelobes are observed to arise in the reconstruction results surrounding the targets. This is owing to the fact that only single frequency sample is utilized to focus the scattered field across all transceiving channels. However, there still exists distinct intensity and distribution variation for the component in non-target regions in above results. Because different probing frequencies exhibit varied propagation patterns when penetrating through layered dielectric media, as a result, the reflectivity and time-delay information of the targets carried

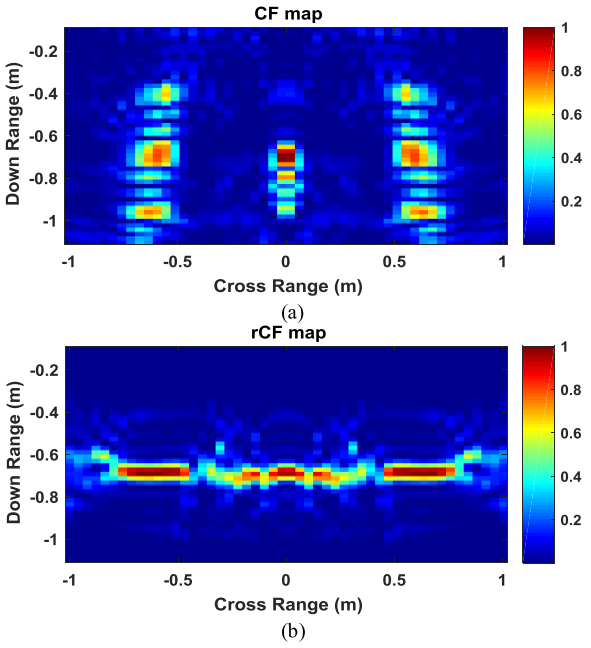

FIGURE 4. Coherence factor map and range coherence factor map for the first simulation example. (a) CF map. (b) rCF map.

in the reflected signals vary slightly for different frequency bins. In other words, down range sidelobes exhibit frequency dependent characteristics across the sub-frequency images. Then, in a similar way, the coherence level measured for the down range sidelobes is expected to be small using equation (7). The resulted rCF map is depicted in Fig. 4 (b), in which the coherence level for the down range sidelobes

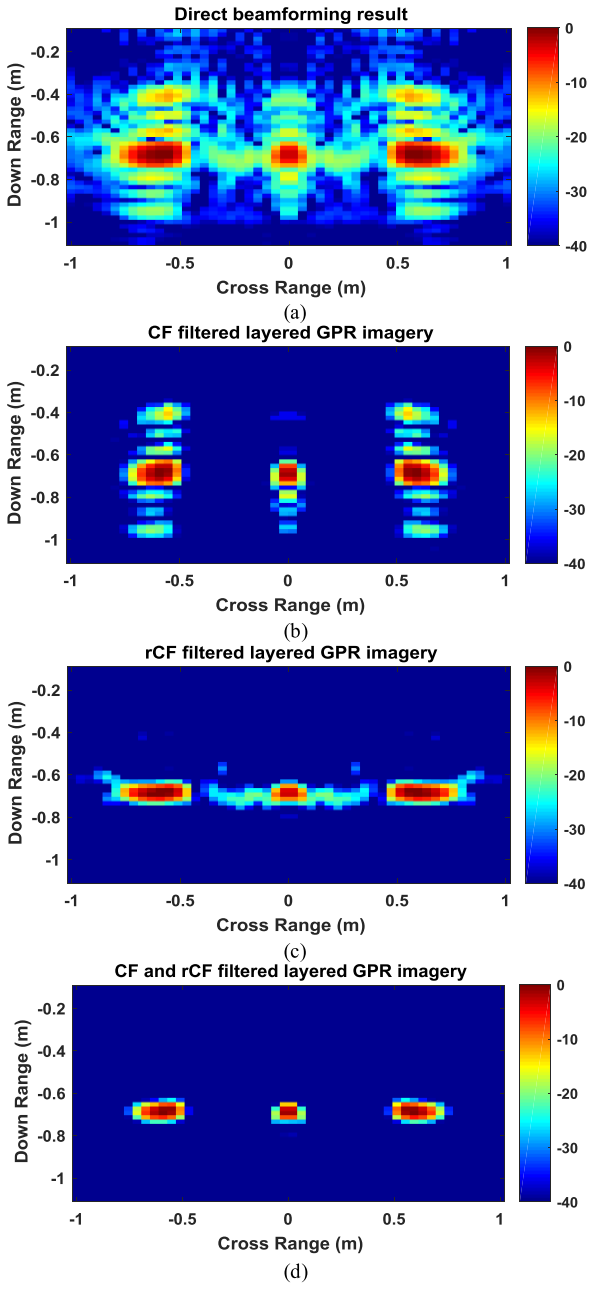

FIGURE 5. Direct imaging result and CF, rCF filter images for three target buried under two layered subsurface ground. (a) Direct beamforming result. (b) CF filtered image. (c) rCF filtered image. (d) Filtered image combining CF and rCF.

is reduced significantly, while that for the grating lobes still remains relatively high. Thus, it should be anticipated that the rCF can suppress the down range sidelobes.

Fig. 5 (a) is the direct reconstructed image for buried targets using inversion scheme in equation (2), in which severe lateral grating lobes and down range sidelobes corrupt the image quality. Fig. 5 (b) is the CF filtered image. The grating lobes are significantly attenuated, while the down range sidelobes still present and relatively strong. This result is in accordance with the theory of CF, which states that only the grating lobes can be suppressed or attenuated. Fig. 5 (c) is the rCF filtered image. The down range sidelobes are completely suppressed, while the residuals of the grating lobes still show up in the image. The result is exactly what the rCF theory aims to achieve. Then, by combining the two-filtering approach together, both the grating lobes and down range sidelobes are effectively suppressed as shown in Fig. 5 (d).

In the second example, we continue to investigate whether the proposed sidelobes suppression technique works for an extended target.

The simulation geometry for radar imaging of a composite target buried under two layered subsurface is depicted as above in Fig. 6. The measurement configuration and operating frequency are the same as in the first example. The dimension of the target is detailed in the schematic geometry in Fig. 6.

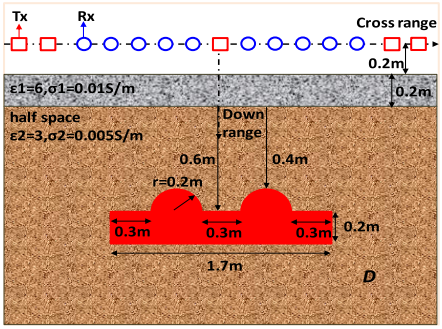

FIGURE 6. Simulation geometry for GPR imaging of a composite target buried under multilayered ground.

Fig. 7 (a) shows the direct beamforming result, in which strong grating lobes and down range sidelobes are observed in the reconstruction result. Fig. 7 (b) shows the CF filtered image. Grating lobes are greatly suppressed while down range sidelobes are not. Fig. 7 (c) shows the rCF filtered image. Down range sidelobes are effectively suppressed as expected while the residuals of the grating lobes are still present. Fig. 7 (d) shows the combinatorial filtered image by employing CF and rCF simultaneously. Both grating lobes and down range sidelobes are significantly suppressed. We note that the discontinuities seen in the reconstructed target profile in the above results, are caused by the blockage of the EM waves by two semicircle components of the composite target.

B. TWRI EXAMPLE

To further illustrate the performance of rCF based down range sidelobes suppression technique, a TWRI imaging example is provided in this part.

The simulation geometry for radar imaging of three targets behind a single layer of wall is shown in Fig. 8. The permittivity and conductivity of the wall are $\varepsilon_r = 6$ and $\sigma = 0.01$ S/m. The thickness of the wall is $d = 0.2$ m. The antenna array configuration and the operating frequency remain the same as in the previous two examples. The only difference in the formulation is to change the half-space subsurface in the above GPR examples to an air layer.

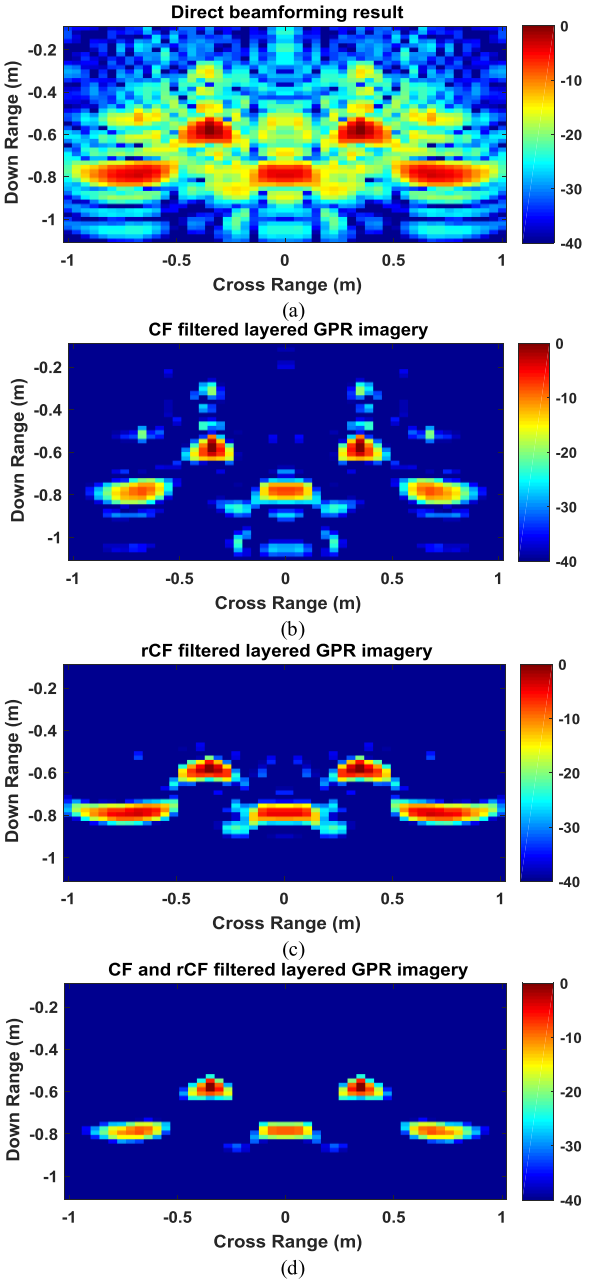

FIGURE 7. Direct imaging result and CF, rCF filtered images for a composite target buried under two layered subsurface ground. (a) Direct beamforming result. (b) CF filtered image. (c) rCF filtered image. (d) Filtered image combining CF and rCF.

Fig. 9 (a) shows the direct imaging result, which is obtained by modifying the subsurface layered Green's function to its far-field approximation in TWRI [31]. Fig. 9 (b) shows the CF filtered image, in which grating lobes are attenuated. Fig. 9 (c) shows the rCF filtered image, in which down range sidelobes are significantly suppressed. Then, in combinatorial filtering result in Fig. 9 (d), a clear image with both grating lobes and down range sidelobes suppression is obtained.

Thus, we could conclude that the proposed rCF technique works not only for GPR imaging but also for TWRI in down range sidelobes suppression. The combinatorial filtering approach is indeed able to achieve the optimal performance by simultaneously suppressing the grating lobes and down range sidelobes.

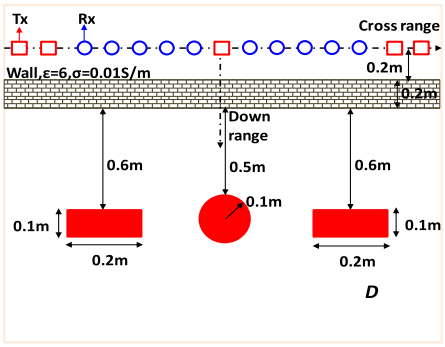

FIGURE 8. Simulation geometry for TWRI imaging of three target buried under multilayered ground.

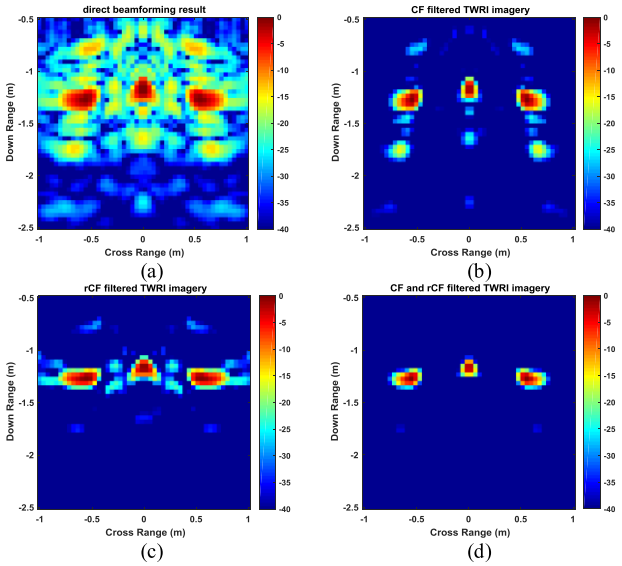

FIGURE 9. Direct imaging result and CF, rCF filtered images for three target obscured behind a single layer of wall. (a) Direct beamforming result. (b) CF filtered image. (c) rCF filtered image. (d) Filtered image combining CF and rCF.

V. EXPERIMENTAL RESULT

In this section, a radar imaging of multiple stationary human targets standing behind a single layer of concrete wall experiment is carried out to verify the effectiveness of the proposed down range sidelobes suppression technique.

The measurement scenario is depicted as in Fig. 10 (a). Three human targets stand stationary behind a single layer of a concrete wall. An antenna system composed of 2 transmitters and 4 receivers spanning an aperture size of 3m is employed to collect the scattered field. The operating frequency of the radar system ranges from 40 MHz to 4.4 GHz with a frequency step of 5 MHz. The onsite measurement scene is as shown in Fig. 10 (b).

Fig. 11 (a) shows the direct focused scene. The reconstruction is completely corrupted by severe grating lobes and clutters. No targets information is observed. Meanwhile,

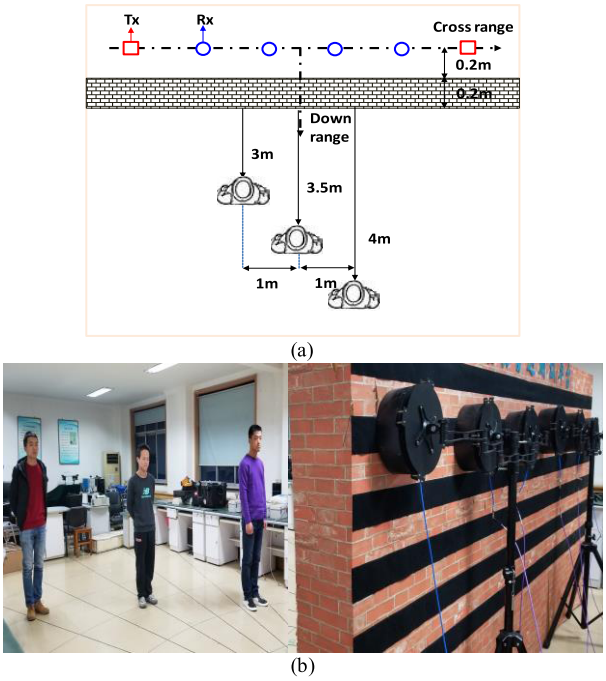

FIGURE 10. Schematic diagram and onsite measurement scenario for radar imaging through a single layer of concrete wall. (a) Schematic diagram. (b) Measurement scenario.

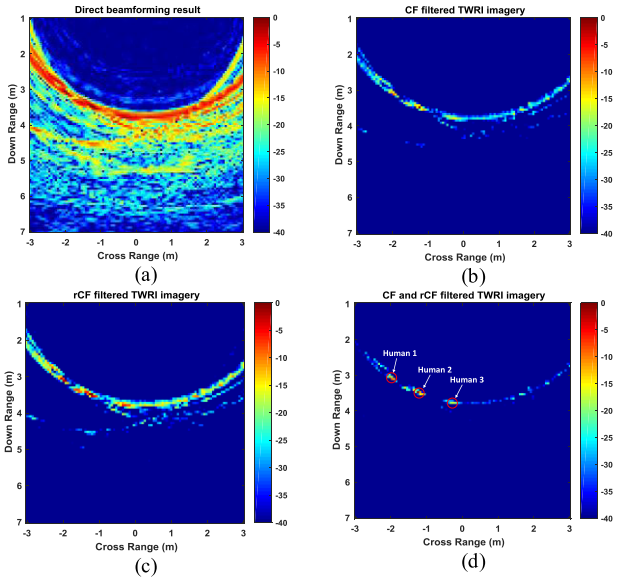

FIGURE 11. Direct imaging result and CF, rCF filtered images for three stationary human targets behind a single layer of wall. (a) Direct beamforming result. (b) CF filtered image. (c) rCF filtered image. (d) Filtered image combining CF and rCF.

the down range sidelobes are not obvious since we have sufficient frequency samples. When CF is applied to filter the image, a very clean image is obtained in Fig. 11 (b), in which the grating lobes and clutters are significantly attenuated. Fig. 11 (c) is the rCF filtered image. Heavy clutters in Fig. 11 (a) are greatly suppressed, while the grating lobes still present themselves rather strongly when compared to the result in Fig. 11 (b). Then, in combinatorial filtering result in Fig. 11 (d), an image with significantly suppressed grating lobes and clutter suppression is achieved. And three behind-the-wall human subjects are clearly highlighted. The reason for the grating lobes residuals in Fig. 11 (b), Fig. 11 (c) and Fig. 11 (d) is due to the fact that an ultra-sparse array is employed in the experiment to sense and image the target space. As expected, even with the aid of proposed combinatorial filtering, the lateral grating lobes cannot be completely suppressed.

VI. CONCLUSIONS

In this paper, an rCF based down range sidelobes suppression technique is proposed for both GPR imaging and TWRI application. We found that grating sidelobes exhibit aspect dependent characteristics, while down range sidelobes exhibit frequency dependent characteristics. The CF filtering can only suppress the grating lobes, while rCF only suppresses the down range sidelobes. Then, by employing a combinatorial filtering strategy, both grating lobes and down range sidelobe can be effectively suppressed. For a real radar imaging application, as for whether to use CF or to use rCF, the authors suggest it should be task specific. For dense arrays, rCF filtering is preferred, while for sparse arrays, CF filtering is preferred. However, no matter what situation one may encounter in practice, the proposed combinatorial or hybrid filtering approach achieves the best performance. The proposed strategy can be readily extended to other microwave imaging applications.

ACKNOWLEDGMENT

The authors would like to thank Shuoguang Wang, Beijing Key Laboratory of Millimeter Wave and Terahertz Technology, Beijing Institute of Technology, for his comments and suggestions to this paper.

REFERENCES

[1] M. G. Amin, *Through-the-Wall Radar Imaging*. Boca Raton, FL, USA: CRC Press, 2014.
[2] H. Jol, *Ground Penetrating Radar Theory and Applications*. Amsterdam, The Netherlands: Elsevier, 2008.
[3] R. Solimene, I. Catapano, G. Gennarelli, A. Cuccaro, A. Dell'Aversano, and F. Soldovieri, "SAR imaging algorithms and some unconventional applications: A unified mathematical overview," *IEEE Signal Process. Mag.*, vol. 31, no. 4, pp. 90–98, Jul. 2014.
[4] G. Gennarelli and F. Soldovieri, "A linear inverse scattering algorithm for radar imaging in multipath environments," *IEEE Geosci. Remote Sens. Lett.*, vol. 10, no. 5, pp. 1085–1089, Sep. 2013.
[5] W. C. Chew, *Waves and Fields in Inhomogeneous Media*. Piscataway, NJ, USA: IEEE Press, 1995.
[6] W. Zhang, A. Hoorfar, and C. Thajudeen, "Building layout and interior target imaging with SAR using an efficient beamformer," in *Proc. IEEE Int. Symp. Antennas Propag. (APSURSI)*, Spokane, WA, USA, Jul. 2011, pp. 2087–2090. doi: 10.1109/APS.2011.5996921.
[7] W. Zhang and A. Hoorfar, "Three-dimensional real-time through-the-wall radar imaging with diffraction tomographic algorithm," *IEEE Trans. Geosci. Remote Sens.*, vol. 51, no. 7, pp. 4155–4163, Jul. 2013.
[8] I. G. Cumming and H. W. Frank, *Digital Processing of Synthetic Aperture Radar Data: Algorithms and Implementation*. Norwood, MA, USA: Artech House, 2005.
[9] H. Lebret and S. Boyd, "Antenna array pattern synthesis via convex optimization," *IEEE Trans. Signal Process.*, vol. 45, no. 3, pp. 526–532, Mar. 1997.

[10] Y. Liu and X. Xu, "Azimuth sidelobe suppression technique for near-field MIMO radar imaging," *Proc. SPIE*, vol. 9643, Oct. 2015, Art. no. 96431E.
[11] J. Tsao and B. D. Steinberg, "Reduction of sidelobe and speckle artifacts in microwave imaging: The CLEAN technique," *IEEE Trans. Antennas Propag.*, vol. 36, no. 4, pp. 543–556, Apr. 1988.
[12] X. Zhuge, A. G. Yarovoy, and L. P. Ligthart, "A sidelobe reduction technique for enhancing images of UWB sparse MIMO array," in *Proc. Int. Radar Conf. (RADAR)*, Bordeaux, France, Oct. 2009, pp. 1–6.
[13] X. Tu, G. Zhu, X. Hu, and X. Huang, "Grating lobe suppression in sparse array-based ultrawideband through-wall imaging radar," *IEEE Antennas Wireless Propag. Lett.*, vol. 15, pp. 1020–1023, 2016.
[14] R. J. Burkholder and K. E. Browne, "Coherence factor enhancement of through-wall radar images," *IEEE Antennas Wireless Propag. Lett.*, vol. 9, pp. 842–845, 2010.
[15] Y. Song, J. Zhu, J. Hu, T. Jin, and Z. Zhou, "Enhanced imaging of building interior for portable MIMO through-the-wall radar," *J. Phys., Conf.*, vol. 960, no. 1, Jan. 2018, Art. no. 012023.
[16] N. S. N. Anwar and M. Z. Abdullah, "Sidelobe suppression featuring the phase coherence factor in 3-D through-the-wall radar imaging," *Radioengineering*, vol. 25, no. 4, pp. 730–740, Dec. 2016.
[17] B. Lu, X. Sun, Y. Zhao, and Z. Zhou, "Phase coherence factor for mitigation of sidelobe artifacts in through-the-wall radar imaging," *J. Electromagn. Waves Appl.*, vol. 27, no. 6, pp. 716–725, Apr. 2013.
[18] J. Camacho, M. Parrilla, and C. Fritsch, "Grating-lobes reduction by application of phase coherence factors," in *Proc. IEEE Int. Ultrason. Symp.*, Rome, Italy, Sep. 2009, pp. 341–344.
[19] J. Liu, Y. Jia, L. Kong, X. Yang, and Q. H. Liu, "Sign-coherence-factor-based suppression for grating lobes in through-wall radar imaging," *IEEE Geosci. Remote Sens. Lett.*, vol. 13, no. 11, pp. 1681–1685, Nov. 2016.
[20] Y. Song, J. Zhu, J. Hu, T. Jin, and Z. Zhou, "Grating lobes suppression for ultra-wideband MIMO radar imaging," in *Proc. 3rd IEEE Int. Conf. Comput. Commun. (ICCC)*, Chengdu, Zhou, Dec. 2017, pp. 957–961.
[21] L. Tan and J. Jiang, *Digital Signal Processing: Fundamentals and Applications*. New York, NY, USA: Academic, 2018.
[22] H. C. Stankwitz, R. J. Dallaire, and J. R. Fienup, "Nonlinear apodization for sidelobe control in SAR imagery," *IEEE Trans. Aerosp. Electron. Syst.*, vol. 31, no. 1, pp. 267–279, Jan. 1995.
[23] X. Tu, G. Zhu, J. Hu, X. Huang, and Z. Zhou, "A sidelobes/grating lobes suppression method for ultrawindeband ultrasparse array through-the-wall imaging radar," in *Proc. IEEE China Summit Int. Conf. Signal Inf. Process. (ChinaSIP)*, Xi'an, China, Jul. 2014, pp. 199–202.
[24] Z. Li, J. Hu, J. Zhang, and G. Zhu, "Sidelobe reduction for UWB radar images based on spatial spectrum segmentation," in *Proc. IEEE 18th Int. Conf. Commun. Technol. (ICCT)*, Chongqing, China, Oct. 2018, pp. 1241–1245.
[25] K. W. Hollman, K. W. Rigby, and M. O'Donnell, "Coherence factor of speckle from a multi-row probe," in *Proc. IEEE Ultrason. Symp.*, vol. 2. Oct. 1999, pp. 1257–1260.
[26] G. Gennarelli, G. Vivone, P. Braca, F. Soldovieri, and M. G. Amin, "Comparative analysis of two approaches for multipath ghost suppression in radar imaging," *IEEE Geosci. Remote Sens. Lett.*, vol. 13, no. 9, pp. 1226–1230, Sep. 2016.
[27] G. Gennarelli and F. Soldovieri, "Multipath ghosts in radar imaging: Physical insight and mitigation strategies," *IEEE J. Sel. Topics Appl. Earth Observ. Remote Sens.*, vol. 8, no. 3, pp. 1078–1086, Mar. 2015.
[28] Y. Jiang, Y. Qin, H. Wang, B. Deng, K. Liu, and B. Cheng, "A sidelobe suppression method based on coherence factor for terahertz array imaging," *IEEE Access*, vol. 6, pp. 5584–5588, 2018.
[29] D. Comite, F. Ahmad, T. Dogaru, and M. G. Amin, "Coherence factor for rough surface clutter mitigation in forward-looking GPR," in *Proc. IEEE Radar Conf. (RadarConf)*, Seattle, WA, USA, May 2017, pp. 1803–1806.
[30] P.-C. Li and M.-L. Li, "Adaptive imaging using the generalized coherence factor," *IEEE Trans. Ultrason., Ferroelectr., Freq. Control*, vol. 50, no. 2, pp. 128–141, Feb. 2003.
[31] W. Zhang and A. Hoorfar, "A generalized approach for SAR and MIMO radar imaging of building interior targets with compressive sensing," *IEEE Antennas Wireless Propag. Lett.*, vol. 14, pp. 1052–1055, 2015.
[32] W. Zhang and A. Hoorfar, "MIMO ground penetrating radar imaging through multilayered subsurface using total variation minimization," *IEEE Trans. Geosci. Remote Sens.*, vol. 57, no. 4, pp. 2107–2115, Apr. 2019. doi: 10.1109/TGRS.2018.2871463.

QIANG AN received the B.E. and M.S. degree from the Department of Biomedical Engineering, Fourth Military Medical University, in 2012 and 2015, respectively. He is currently pursuing the Ph.D. degree with the Department of Biomedical Engineering, Fourth Military Medical University. He was with the Antenna Research Laboratory, Center for Advanced Communication, Villanova University, as a joint training Ph.D. Student under the supervisor of Dr. A. Hoorfar, from 2017 to 2018. His research interests include inverse scattering methods and compressed sensing with structured priors applied to through-the-wall radar imaging, and ground penetrating radar imaging applications.

AHMAD HOORFAR (S'78–M'84–SM'95) received the B.S. degree in electronics engineering from the University of Tehran, in 1975, and the M.S. and Ph.D. degrees in electrical engineering from the University of Colorado at Boulder, in 1978 and 1984, respectively.

Before joining Villanova University, in 1988, he was a Postdoctoral Research Fellow with the Electromagnetics Laboratory, University of Colorado, from 1984 to 1986, and a Research Faculty Member with the NSF Research Center for Microwave/Millimeter-Waves Computer-Aided Design (MIMICAD), Boulder, from 1986 to 1988. He is currently a Professor of electrical and computer engineering, the Director of the Antenna Research Laboratory, and the Program Director of the EE Department's graduate admission and advising at Villanova University. He spent his sabbatical leaves, in 2002 and 2009, at the NASA's Jet Propulsion Laboratory (JPL) in Pasadena, CA, USA, where he contributed to the development of various global optimization techniques for the design of feed horns and antennas for the NASA's deep space communication network. His current research interests include electromagnetic field theory, electrically small and ultra-wideband antennas, metamaterials, microwave sensing and imaging, radar systems, and evolutionary computational methods. He is a member of the Franklin Institute's Committee on Science and the Arts and the URSI, commission B. In 1995, he was a recipient of the Philadelphia Section "IEEE Chapter of the Year Award" for his leadership in chairing the AP/MTT joint chapter, from 1993 to 1995. He was a recipient of the Outstanding Faculty Research Scholar Award from Villanova University, in 2007. He has organized numerous special sessions and has been an invited speaker at various international symposia in these areas. He was the General Chair and an Organizer of the 12th and 13th Benjamin Franklin Symposia in Microwave and Antenna Technology held, in 1994 and 1995 and the Co-Organizer of the 22nd Antenna Measurement Technique Association (AMTA) Symposium, in 2000. He has served as a Reviewer for various IEEE and other technical publications on antennas and microwaves in the last 30 years. He has also been on the technical program committees of numerous international symposia and conferences, including the IEEE AP-S, IEEE Aerospace, IEEE Radio and Wireless, IEEE Radar Conference, International Union of Radio Science (URSI), and Progress in Electromagnetic Research Symposia.

WENJI ZHANG received the B.S. degree from the Huazhong University of Science and Technology (HUST), Wuhan, China, in 2004, and the Ph.D. degree in electrical engineering from the Institute of Electronics, Chinese Academy of Sciences (CAS), Beijing, China, in 2009. From 2009 to 2011, he was with the Antenna Research Laboratory, Villanova University, Villanova, PA, USA, as a Postdoctoral Research Fellow. He was with the Department of Electrical and Computer Engineering, Duke University, Durham, NC, USA, first as a Postdoctoral Associate and then as a Research Scientist. His research interests include 5G millimeter-wave technology, antennas and wave propagation, electromagnetic inverse scattering, radar imaging, electromagnetic methods in geophysics, and compressive sensing.

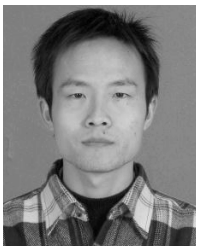

SHIYONG LI (M'17) received the B.S. degree in electrical engineering from Shandong University, Jinan, China, in 2002, and the Ph.D. degree in electromagnetic field and microwave technology from the Beijing Institute of Technology, Beijing, China, in 2008. From 2009 to 2010, he was a Postdoctoral Researcher with the School of Electronics Engineering and Computer Science, Peking University, Beijing. Since 2010, he has been with the Faculty of the School of Information and Electronics, Beijing Institute of Technology, where he is currently an Associate Professor. He was a Visiting Research Scholar with the Center for Advanced Communications, Villanova University, Villanova, PA, USA. His current research interests include microwave imaging and compressive sensing.

JIANQI WANG was born in Xi'an, Shaanxi, China, in 1962. He received the B.E. degree in information and control engineering from Xi'an Jiaotong University, Xi'an, in 1984, the M.E. degree in electronic engineering from the National University of Defense Technology, Changsha, China, in 1990, and the Ph.D. degree from the Key Laboratory of the Ministry of Education of China, Xi'an Jiaotong University, in 2006. Since 1990, he has taught at the School of Biomedical Engineering, Fourth Military Medical University, Xi'an, where he is currently a Professor and the Director of the Department of Electronics. He pioneered radar-based human being detection in China, in 1998, and has published more than 100 articles on the technology. His research interests include bioradar technology, including signal processing, human being detection, and imaging.